

Tensor Learning and Compression of N-phonon Interactions

Yao Luo,¹ Dhruv Mangtani,¹ Shiyu Peng,¹ Jia Yao,¹ Sergei Kliavinek,¹ and Marco Bernardi¹

¹*Department of Applied Physics and Materials Science, and Department of Physics,
California Institute of Technology, Pasadena, California 91125, USA*

Phonon interactions from lattice anharmonicity govern thermal properties and heat transport in materials. These interactions are described by n -th order interatomic force constants (n -IFCs), which can be viewed as high-dimensional tensors correlating the motion of n atoms, or equivalently encoding n -phonon scattering processes in momentum space. Here, we introduce a tensor decomposition to efficiently compress n -IFCs for arbitrary order n . Using tensor learning, we find optimal low-rank approximations of n -IFCs by solving the resulting optimization problem. Our approach reveals the inherent low dimensionality of phonon-phonon interactions and allows compression of the 3 and 4-IFC tensors by factors of up to $10^3 - 10^4$ while retaining high accuracy in calculations of phonon scattering rates and thermal conductivity. Calculations of thermal conductivity using the compressed n -IFCs achieve a speed-up by nearly three orders of magnitude with $>98\%$ accuracy relative to the reference uncompressed solution. These calculations include both 3- and 4-phonon scattering and are shown for a diverse range of materials (Si, HgTe, MgO, and TiNiSn). In addition to accelerating state-of-the-art thermal transport calculations, the method shown here paves the way for modeling strongly anharmonic materials and higher-order phonon interactions.

Phonon-phonon (ph-ph) interactions are crucial to understanding thermal transport, lattice dynamics, and structural phase transitions in condensed matter [1]. They originate from the anharmonicity of the lattice potential and can be described by n -th order interatomic force constant (n -IFC) tensors, where $n \geq 3$. Density function theory (DFT) [2] calculations combined with fitting algorithms provide accurate n -IFC tensors [3–6], enabling quantitative predictions of thermal transport in materials [7–12]. However, the high-dimensionality of the IFC tensors obscures the underlying physics and poses significant computational challenges. The complexity of n -phonon (n -ph) interactions grows exponentially with order n , a clear example of the curse of dimensionality. For thermal conductivity calculations, 4-ph interactions require orders of magnitude more computational effort than 3-ph interactions, whereas 5-ph and higher-order ph-ph interactions remain inaccessible.

To overcome this complexity, discovering low-rank approximations of n -IFC could be game changing. There is growing interest in such dimensionality reduction approaches, including tensor network states for many-body wave functions [13, 14], tensor train for differential equations [15–17] and Feynman diagrams [16, 18], tensor hyper-contraction [19–21] and density fitting [22] for electron interactions in quantum chemistry, and feature optimization for atomic machine learning [23–26]. Recent work has employed singular value decomposition to compress electron-phonon (e -ph) interactions and greatly speed up first-principles e -ph calculations [27]. For ph-ph interactions, previous work has taken advantage of crystal symmetry to reduce the number of free parameters and compute the n -IFCs with fewer DFT force calculations [28]. The compressed sensing technique has also been used to obtain n -IFCs using sparse solvers [4, 29]. However, in previous work the n -IFCs are still stored and

handled explicitly in full tensor form, Φ_{ijk} and Φ_{ijkl} for 3- and 4-IFCs respectively, and a low-rank representation of n -IFCs is still missing.

In this Letter, we introduce a low-rank tensor ansatz for n -ph interactions in momentum space based on the CANDECAMP/PARAFAC (CP) decomposition [30], a compression method used in tensor learning [31–33]. The proposed ansatz is a permanent CP (PCP) decomposition, which generalizes the CP decomposition to enforce bosonic statistics. To find an optimal low-rank PCP decomposition, we formulate the tensor learning problem and solve it on GPU hardware. The optimized low-rank PCP tensors achieve large compression factors of $10^3 - 10^4$ with minimal compression losses of only a few percent in all materials we study. This result reveals the inherent low-dimensionality of n -ph interactions and enables a speedup of nearly three orders of magnitude for calculations using n -IFCs, including phonon relaxation times and thermal conductivity. We also introduce constraints to treat ph-ph interactions for long-wavelength acoustic phonons, leading to nearly lossless predictions of thermal conductivity compared to calculations using full n -IFC tensors. Finally, we show that the PCP ansatz can uncover dominant modes in n -ph interactions, providing a valuable tool for understanding microscopic thermal transport mechanisms and formulating accurate minimal models. Beyond ph-ph interactions, the PCP ansatz and corresponding open-source routines developed here provide a blueprint for modeling momentum-dependent tensors, with broad applications in condensed matter physics.

We consider the n -ph interaction $V^{(n)}(\mathbf{Q}_1, \dots, \mathbf{Q}_n)$, which describes the scattering amplitude of n phonon modes. Each mode is specified by a wave vector \mathbf{q}_i and branch index ν_i , collectively denoted as $\mathbf{Q}_i = (\nu_i, \mathbf{q}_i)$ for $i = 1, \dots, n$. For instance, the 3-ph interaction is given

by

$$V^{(3)}(\mathbf{Q}_1, \mathbf{Q}_2, \mathbf{Q}_3) = \delta \left(\sum_{i=1}^3 \mathbf{q}_i \right) \sum_{b_1, l_2 b_2, l_3 b_3} \sum_{\alpha_1 \alpha_2 \alpha_3} \times \Phi_{0b_1, l_2 b_2, l_3 b_3}^{\alpha_1, \alpha_2, \alpha_3} \frac{e_{\alpha_1 b_1}^{\mathbf{Q}_1} e_{\alpha_2 b_2}^{\mathbf{Q}_2} e_{\alpha_3 b_3}^{\mathbf{Q}_3}}{\sqrt{m_{b_1} m_{b_2} m_{b_3}}} e^{i\mathbf{q}_2 \mathbf{r}_{l_2} + i\mathbf{q}_3 \mathbf{r}_{l_3}}, \quad (1)$$

where each of the l , b , and α label the primitive cell, atom, and Cartesian coordinate, respectively; $e_{\alpha b}^{\mathbf{Q}}$ is the displacement eigenvector of phonon mode \mathbf{Q} , m_b is the mass of atom b , and \mathbf{r}_l is the position of primitive cell l . Above, $\Phi_{0b, l_1 b_1, l_2 b_2}^{\alpha, \alpha_1, \alpha_2}$ is the 3-IFC tensor associated with three atomic displacements, the first displacement fixed at the cell origin. For general n -ph interactions, analogous n -IFC tensors $\Phi^{(n)}$ can be defined.

To compress the n -ph interactions $V^{(n)}$, we propose the PCP decomposition as the low-rank ansatz

$$\tilde{V}^{(n)}(\mathbf{Q}_1, \dots, \mathbf{Q}_n) = \delta \left(\sum_{i=1}^n \mathbf{q}_i \right) \times \sum_{\xi=1}^{N_c^{(n)}} \frac{\lambda_\xi}{n!} \sum_{\sigma \in S_n} A_1^\xi(\mathbf{Q}_{\sigma_1}) A_2^\xi(\mathbf{Q}_{\sigma_2}) \dots A_n^\xi(\mathbf{Q}_{\sigma_n}), \quad (2)$$

where $N_c^{(n)}$ is the PCP rank, λ_ξ the ξ -th PCP singular value, A_i^ξ are the corresponding PCP modes, and S_n is the symmetric group of order n containing all the permutations of $(1, \dots, n)$. Note that Eq. (2) correctly preserves the bosonic exchange symmetry and momentum conservation of n -ph interactions. For $N_{\mathbf{Q}}$ phonon modes, storing 3-ph interactions $V^{(3)}$ requires $\mathcal{O}(N_{\mathbf{Q}}^2)$ resources versus $\mathcal{O}(3N_c^{(3)} N_{\mathbf{Q}})$ for its PCP compressed counterpart $\tilde{V}^{(3)}$. This yields a large storage reduction, by a factor of $N_{\mathbf{Q}}/(3N_c^{(3)}) \approx 10^3$ – 10^4 in a typical calculation.

Since $V^{(n)}$ is obtained by transforming the n -IFC $\Phi^{(n)}$ to momentum space, we derive the corresponding low-rank ansatz for 3- and 4-IFCs in real space:

$$\tilde{\Phi}_{l_1 b_1, l_2 b_2, l_3 b_3}^{\alpha_1, \alpha_2, \alpha_3} = \sum_{\xi=1}^{N_c^{(3)}} \frac{\lambda_\xi}{3!} \sum_{\sigma \in S_3} \sum_l \prod_{i=1}^3 A_{\sigma_i}^\xi(l_i - l, b_i \alpha_i), \quad (3)$$

$$\tilde{\Phi}_{l_1 b_1, l_2 b_2, l_3 b_3, l_4 b_4}^{\alpha_1, \alpha_2, \alpha_3, \alpha_4} = \sum_{\xi=1}^{N_c^{(4)}} \frac{\lambda_\xi}{4!} \sum_{\sigma \in S_4} \sum_l \prod_{i=1}^4 B_{\sigma_i}^\xi(l_i - l, b_i \alpha_i),$$

where $A_i^\xi(l, b\alpha)$ is the real-space representation of $A_i^\xi(\mathbf{Q})$, $A_i^\xi(\mathbf{Q}) = \sum_{l, b\alpha} \frac{e_{b\alpha}^{\mathbf{Q}}}{\sqrt{m_b}} e^{i\mathbf{q}\mathbf{r}_l} A_i^\xi(l, b\alpha)$. To enforce the acoustic sum rule [28], we impose $\sum_{l, b} A_i^\xi(l, b\alpha) = 0$. Derivations for generic n -IFCs and their PCP decomposition are provided in the Supplemental Material (SM) [34]. The computational cost of PCP-compressed $\tilde{\Phi}^{(n)}$ and $\tilde{V}^{(n)}$ scales linearly with system size, making it promising for calculations in complex materials with large unit cells.

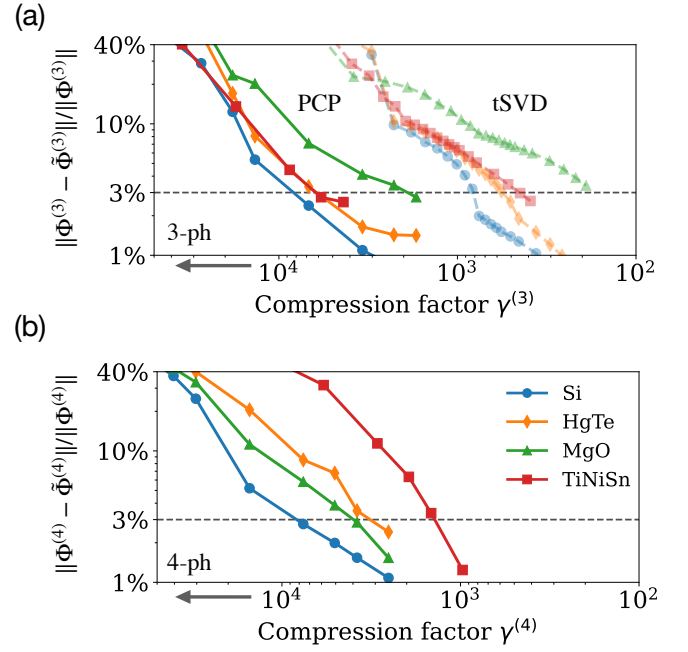


FIG. 1. Relative compression loss vs. compression factor $\gamma^{(n)}$. (a) Results for 3-IFC tensors comparing PCP (solid lines) and tSVD (dashed lines). (b) Results for 4-IFC tensors. The compression factor $\gamma^{(n)}$ is defined in Eq. (5).

To find optimal PCP modes A_i^ξ (or B_i^ξ) that best approximate the original IFC tensors $\Phi^{(n)}$ computed with DFT, we minimize the loss function:

$$L = \|\tilde{\Phi}^{(n)}[\mathbf{A}] - \Phi^{(n)}\|^2, \quad (4)$$

where $\tilde{\Phi}^{(n)}$ is the low-rank IFC tensor in Eq. (3), and the norm is defined as $\|\mathbf{x}\| = \sqrt{\sum_I x_I^2}$ [35]. This is a typical tensor learning problem that lacks closed-form solutions for high-order tensors. In addition, existing optimization algorithms are computationally demanding for large tensors. We address this challenge by developing a computational toolkit, called PHONON-PCP, implemented using PYTORCH [36]. This optimization routine follows a standard “neural network”-like training loop, where $\tilde{\Phi}^{(n)}$ is evaluated in a forward pass, and A_i^ξ is the learnable weight trained using automatic differentiation. A typical optimization involves 10^3 – 10^4 trainable parameters, depending on the material. The algorithm runs efficiently on GPUs – the compression process for one material converges in one hour on a single NVIDIA A100 chip.

We apply our approach to four materials: Si, HgTe, MgO and TiNiSn. For each material, we generate force-displacement datasets from DFT force calculations on supercells and then employ ALAMODE [3] to extract the 3- and 4-IFCs. We include 3-IFCs up to the fifth-nearest neighbors and 4-IFCs up to the second-nearest neighbors for Si, HgTe and MgO. For TiNiSn, the 3-IFCs are truncated to 6.4 Å and the 4-IFCs to 3.8 Å. We calculate DFT forces using VASP [37, 38] with PBEsol functional [39].

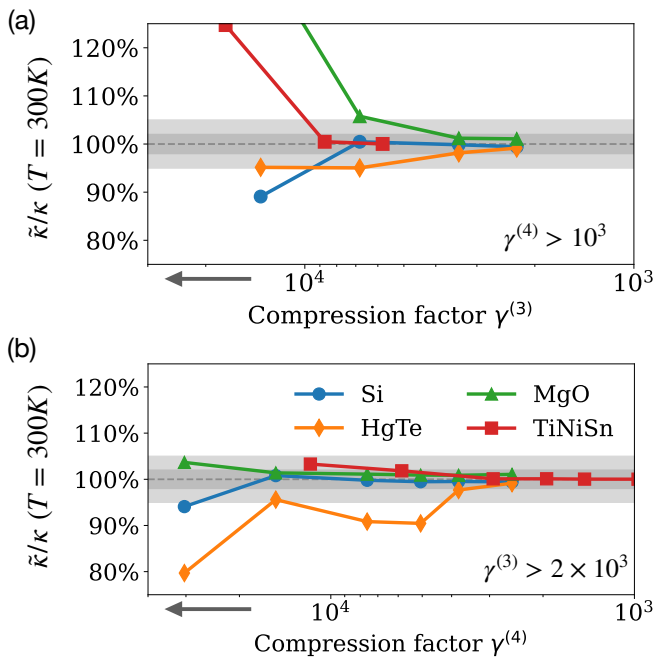


FIG. 2. Ratio of the thermal conductivity $\tilde{\kappa}$, computed using compressed 3- and 4-ph interactions, to the thermal conductivity κ computed with uncompressed tensors. Results are shown as a function of: (a) 3-ph compression factor, $\gamma^{(3)}$, for fixed $\gamma^{(4)} > 10^3$ ($N_c^{(4)} = 48$), and (b) 4-ph compression factor, $\gamma^{(4)}$, for fixed $\gamma^{(3)} > 2 \times 10^3$ ($N_c^{(3)} = 24$). The light (dark) shaded regions show the 95% (98%) accuracy windows.

For polar materials, we calculate Born effective charges using density functional perturbation theory in VASP, and use the Ewald summation to compute the nonanalytic part of the dynamical matrix [40]. Additional computational details are provided in the SM [34].

To assess the accuracy of PCP for compressing n -ph interactions, we calculate the error relative to uncompressed n -IFCs, expressed as the compression loss $\|\tilde{\Phi}^{(n)} - \Phi^{(n)}\|/\|\Phi^{(n)}\|$, as a function of the compression factor $\gamma^{(n)}$, which quantifies parameter reduction in the n -IFCs:

$$\gamma^{(n)} = \frac{\# \text{ of nonzero entries of } \Phi^{(n)}}{N_c^{(n)}}. \quad (5)$$

This error analysis is shown for the 3-ph interactions in Fig. 1(a). We achieve compression factors of 10^3 – 10^4 at the 3% compression error threshold. For comparison, a truncated singular value decomposition (tSVD) of 3-ph interactions, inspired by our previous work on e -ph coupling [27], can only reach compression factors of a few hundred for the same 3% compression loss. Therefore, the PCP approach provides a 10-times more favorable dimensionality reduction than SVD for all materials we study. We attribute the superior performance of PCP to its flexible ansatz combined with the correct permutation symmetry and the explicit parameter optimization

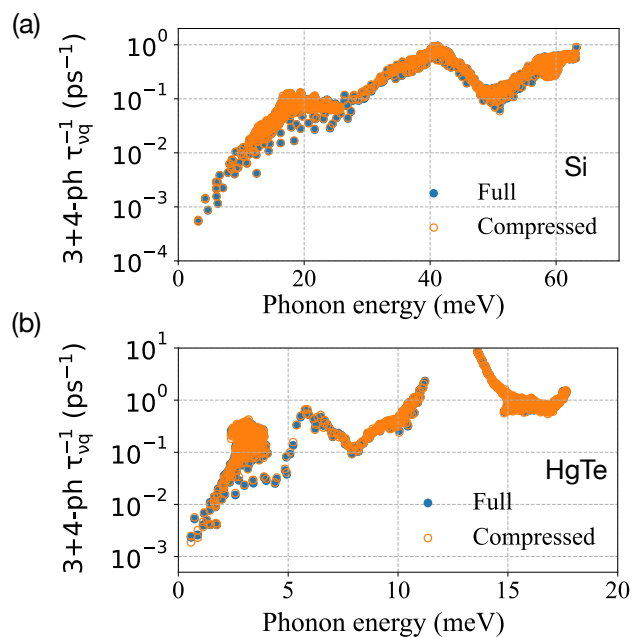


FIG. 3. Phonon scattering rates combining 3- and 4-ph interactions, shown as a function of phonon energy for (a) Si and (b) HgTe, comparing results for full IFC tensors (blue dots) and compressed IFC tensors (orange circles). In both materials, we show results for compression factors $\gamma^{(3)} = 2200$ for 3-ph, and $\gamma^{(4)} = 2500$ for 4-ph interactions.

during tensor learning, which enable effective low-rank representation of n -ph interactions. We achieve similarly large compression factors for 4-ph interactions, as shown in Fig. 1(b). These results highlight the inherent low-dimensionality of n -ph interactions, and show their accurate low-rank approximation using tensor learning.

Using compressed n -ph interactions, we compute the thermal conductivity at 300 K for the four materials. Our calculations use the single-mode relaxation time approximation [7, 41, 42] and include both 3- and 4-ph interactions [43–46] with a converged number of scattering processes (2×10^5) for 3- and 4-ph scattering rates [47] (see details in SM [34]). The thermal conductivity $\tilde{\kappa}$, computed with compressed n -IFC tensors, is compared with the reference value κ from full (uncompressed) tensors in Fig. 2(a) and (b). We find that $\tilde{\kappa}$ converges to the reference value for large compression factors, $\gamma^{(3)} \approx 7 \times 10^3$ and $\gamma^{(4)} \approx 10^4$ for Si, MgO, and TiNiSn, and slightly smaller $\gamma^{(4)} = 3 \times 10^3$ for HgTe, where the 4-ph contribution is more important [9]. Even for these very large compression factors, the approximate thermal conductivity is still within 2% of the reference value obtained with full IFCs [34]. This high accuracy for thermal conductivity is a result of the low compression losses for n -IFCs.

We also examine the accuracy of compressed IFC tensors for calculating the microscopic scattering rate for each phonon mode, $\tau_{\nu\mathbf{q}}^{-1}$. In Figs. 3(a) and (b), the phonon scattering rates from compressed IFC tensors are

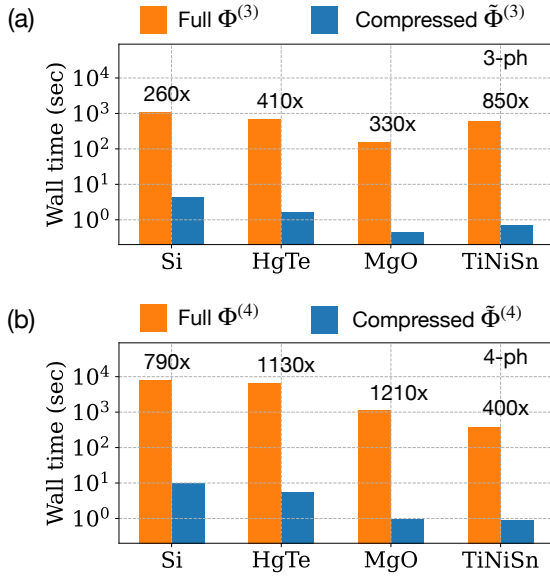


FIG. 4. Comparison of computational cost (CPU wall time) for calculations using compressed and full IFC tensors. Results are shown for (a) 3-ph scattering rates with compression factors $\gamma^{(3)} > 2200$ and (b) 4-ph scattering rates with compression factors $\gamma^{(3)} > 2500$ in all materials. The speedup achieved with compressed tensors is given in figure for each material.

nearly identical to those from full IFC tensors for each single phonon mode, even in cases where $\tau_{\nu q}^{-1}$ varies by up to four orders of magnitude over the phonon spectrum. We calculate the coefficient of determination R^2 [48] between approximate and reference $\tau_{\nu q}^{-1}$, and find values of $R^2 = 0.9996$ for Si and $R^2 = 0.9986$ for HgTe, further confirming the accuracy of the compressed n -ph interactions. The approximate scattering rates achieve a similar accuracy in TiNiSn and MgO [34].

The dimensionality reduction provided by PCP leads to massive cost savings for calculations involving n -ph interactions, with speed-up proportional to the compression factor (see analysis in SM [34]). In Fig. 4, we compare CPU wall times for calculations of 3-ph and 4-ph scattering rates using full and compressed n -IFCs with large compression factors ($\gamma^{(3)} > 2200$ and $\gamma^{(4)} > 2500$). For all materials studied here, the use of compressed IFC tensors enables a speed-up of 260–1210 in calculations of thermal conductivity. Calculations of $\tau_{\nu q}^{-1}$ using compressed IFC tensors are so efficient that computing the thermal conductivity with 3- and 4-ph interactions takes less than half a minute for each material studied here. Using compressed IFC tensors, we are able to accurately extrapolate the thermal conductivity to the thermodynamic limit (TDL) by employing progressively denser momentum grids. The importance of extrapolating to the TDL is clear from the case of HgTe, where the TDL-extrapolated κ is 47% larger than the value obtained with reasonable grid sizes of 16^3 [34]. The calculation for the largest grid, 250^3 , requires only 2.5 CPU node-hours.

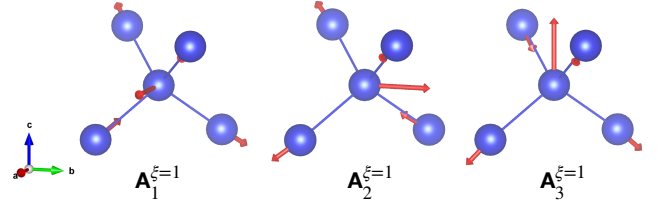


FIG. 5. The PCP mode triplet $A_{i=1,2,3}^{\xi=1}$ with the largest 3-ph coupling strength in Si. The three modes are related by the C_3 rotation symmetry along the [111] direction in Si.

The PCP decomposition also offers interesting ways to analyze n -ph interactions. We express the n -ph anharmonic energy $E^{(n)}(\mathbf{u})$ in terms of PCP modes [34],

$$E^{(n)}(\mathbf{u}) = \sum_l \sum_{\xi} \frac{\lambda_{\xi}}{n!} \prod_{i=1}^n \phi_i^{\xi}(l, \mathbf{u}), \quad (6)$$

$$\begin{aligned} \phi_i^{\xi}(l, \mathbf{u}) &= \langle \mathbf{A}_i^{\xi}(l), \mathbf{u} \rangle \\ &= \sum_{l'b\alpha} A_{\sigma_i}^{\xi}(l' - l, b\alpha) u(l'b\alpha), \end{aligned} \quad (7)$$

where $u(lb\alpha)$ is the displacement of atom b in primitive cell l along the α direction. Here, the PCP modes $[\mathbf{A}_i^{\xi}(l)]_{l'b\alpha} = A_{\sigma_i}^{\xi}(l' - l, b\alpha)$ are viewed as local vibrational modes, centered in the l -th primitive cell, which give dominant contributions the n -th order anharmonic energy $E^{(n)}(\mathbf{u})$. Therefore, the projection $\phi_i^{\xi}(l, \mathbf{u})$ defined in Eq. (7) is a descriptor of the atomic environment that quantifies the similarity between the local atomic displacement \mathbf{u} and the PCP modes $\mathbf{A}_i^{\xi}(l)$. (Interestingly, the anharmonic energy for PCP decomposition in Eq. (6) has a structure similar to the slave mode [49, 50] and the atomic cluster expansion models [51].)

In Fig. 5, we visualize the three modes associated with the largest PCP singular value for 3-ph interactions in Si. The PCP-mode triplet $\{\mathbf{A}_1^{\xi=1}, \mathbf{A}_2^{\xi=1}, \mathbf{A}_3^{\xi=1}\}$ provides the best rank-1 approximation of 3-IFC tensors in Si and is obtained by setting the PCP rank to $N_c^{(3)} = 1$ in the training process. These three modes are related by a C_3 rotation along the [111] crystal direction:

$$\hat{C}_3 \mathbf{A}_1^{\xi=1} = \mathbf{A}_2^{\xi=1}, \quad \hat{C}_3 \mathbf{A}_2^{\xi=1} = \mathbf{A}_3^{\xi=1}, \quad \hat{C}_3 \mathbf{A}_3^{\xi=1} = \mathbf{A}_1^{\xi=1}.$$

Even though we do not explicitly preserve the space-group symmetry when generating the PCP modes, the rank-1 PCP ansatz is capable of learning the C_3 symmetry of Si encoded in the uncompressed 3-IFC tensors during the optimization process. In general, the space-group symmetry is preserved in the compressed IFCs, with only a small symmetry loss resulting from compression (see SM [34]).

In summary, we propose a tensor decomposition of n -ph interactions and show compression of n -IFC tensors using GPU-accelerated tensor learning. Our PCP

decomposition reveals the inherent low-dimensionality of 3- and 4-ph interactions in crystals, enabling compression factors greater than 10^3 for minimal compression errors of less than 3%. We achieve corresponding cost savings for calculations of phonon scattering rates and thermal conductivity. The large speed-up makes our method suitable for high-throughput screening of thermal transport in materials and offers a promising pathway to go beyond 3- and 4-ph interactions. The PCP decomposition can also uncover dominant atomic environment descriptors, providing valuable information for formulating machine learning atomic force fields. Future work will explore 5-ph and higher n -ph interactions in strongly anharmonic materials, use PCP to obtain simplified coupled-mode equations for nonlinear phonon processes, and accelerate simulations of ultrafast phonon dynamics.

Y.L. thanks Junjie Yang for fruitful discussions. This work was supported by the National Science Foundation under Grant No. OAC-2209262. Y.L. acknowledges support from the Eddleman Fellowship. This research used resources of the National Energy Research Scientific Computing Center, a DOE Office of Science User Facility supported by the Office of Science of the U.S. Department of Energy under Contract No. DE-AC02-05CH11231 using NERSC award NERSC DDR-ERCAP0026831.

- [1] M. Born and K. Huang, *Dynamical Theory of Crystal Lattices* (Oxford University Press, 1996).
- [2] R. M. Martin, *Electronic Structure: Basic Theory and Practical Methods* (Cambridge University Press, 2004).
- [3] T. Tadano, Y. Gohda, and S. Tsuneyuki, Anharmonic force constants extracted from first-principles molecular dynamics: applications to heat transfer simulations, *J. Condens. Matter Phys.* **26**, 225402 (2014).
- [4] F. Zhou, W. Nielson, Y. Xia, and V. Ozoliņš, Lattice anharmonicity and thermal conductivity from compressive sensing of first-principles calculations, *Phys. Rev. Lett.* **113**, 185501 (2014).
- [5] O. Hellman and I. A. Abrikosov, Temperature-dependent effective third-order interatomic force constants from first principles, *Phys. Rev. B* **88**, 144301 (2013).
- [6] A. H. Romero, E. K. U. Gross, M. J. Verstraete, and O. Hellman, Thermal conductivity in pbte from first principles, *Phys. Rev. B* **91**, 214310 (2015).
- [7] D. A. Broido, M. Malorny, G. Birner, N. Mingo, and D. A. Stewart, Intrinsic lattice thermal conductivity of semiconductors from first principles, *Appl. Phys. Lett.* **91**, 231922 (2007).
- [8] N. K. Ravichandran and D. Broido, Phonon-phonon interactions in strongly bonded solids: Selection rules and higher-order processes, *Phys. Rev. X* **10**, 021063 (2020).
- [9] Y. Xia, V. I. Hegde, K. Pal, X. Hua, D. Gaines, S. Patel, J. He, M. Aykol, and C. Wolverton, High-throughput study of lattice thermal conductivity in binary rocksalt and zinc blende compounds including higher-order anharmonicity, *Phys. Rev. X* **10**, 041029 (2020).
- [10] J. Carrete, W. Li, N. Mingo, S. Wang, and S. Curtarolo, Finding unprecedentedly low-thermal-conductivity half-heusler semiconductors via high-throughput materials modeling, *Phys. Rev. X* **4**, 011019 (2014).
- [11] W. Li, J. Carrete, N. A. Katcho, and N. Mingo, Sheng-BTE: a solver of the Boltzmann transport equation for phonons, *Comp. Phys. Commun.* **185**, 1747–1758 (2014).
- [12] G. Barbalinardo, Z. Chen, N. W. Lundgren, and D. Donadio, Efficient anharmonic lattice dynamics calculations of thermal transport in crystalline and disordered solids, *J. Appl. Phys.* **128**, 135104 (2020).
- [13] J. I. Cirac, D. Pérez-García, N. Schuch, and F. Verstraete, Matrix product states and projected entangled pair states: Concepts, symmetries, theorems, *Rev. Mod. Phys.* **93**, 045003 (2021).
- [14] R. Orús, A practical introduction to tensor networks: Matrix product states and projected entangled pair states, *Ann. Phys.* **349**, 117 (2014).
- [15] I. V. Oseledets, Tensor-train decomposition, *SIAM J. Sci. Comput.* **33**, 2295 (2011).
- [16] Y. Núñez Fernández, M. Jeannin, P. T. Dumitrescu, T. Kloss, J. Kaye, O. Parcollet, and X. Waintal, Learning feynman diagrams with tensor trains, *Phys. Rev. X* **12**, 041018 (2022).
- [17] R. D. Peddinti, S. Pisoni, A. Marini, P. Lott, H. Argenterieri, E. Tiunov, and L. Aolita, Quantum-inspired framework for computational fluid dynamics, *Commun. Phys.* **7**, 135 (2024).
- [18] H. Shinaoka, M. Wallerberger, Y. Murakami, K. Nogaki, R. Sakurai, P. Werner, and A. Kauch, Multiscale space-time ansatz for correlation functions of quantum systems based on quantics tensor trains, *Phys. Rev. X* **13**, 021015 (2023).
- [19] E. G. Hohenstein, R. M. Parrish, and T. J. Martínez, Tensor hypercontraction density fitting. i. quartic scaling second- and third-order möller-pleiset perturbation theory, *J. Chem. Phys.* **137**, 044103 (2012).
- [20] R. M. Parrish, E. G. Hohenstein, T. J. Martínez, and C. D. Sherrill, Tensor hypercontraction. ii. least-squares renormalization, *J. Chem. Phys.* **137**, 224106 (2012).
- [21] E. G. Hohenstein, R. M. Parrish, C. D. Sherrill, and T. J. Martínez, Communication: Tensor hypercontraction. iii. least-squares tensor hypercontraction for the determination of correlated wavefunctions, *J. Chem. Phys.* **137**, 221101 (2012).
- [22] B. I. Dunlap, Robust and variational fitting, *Phys. Chem. Chem. Phys.* **2**, 2113 (2000).
- [23] M. J. Willatt, F. Musil, and M. Ceriotti, Feature optimization for atomistic machine learning yields a data-driven construction of the periodic table of the elements, *Phys. Chem. Chem. Phys.* **20**, 29661 (2018).
- [24] G. Imbalzano, A. Anelli, D. Giofré, S. Klees, J. Behler, and M. Ceriotti, Automatic selection of atomic fingerprints and reference configurations for machine-learning potentials, *J. Chem. Phys.* **148**, 241730 (2018).
- [25] R. K. Cersonsky, B. A. Helfrecht, E. A. Engel, S. Klavinek, and M. Ceriotti, Improving sample and feature selection with principal covariates regression, *Mach. Learn.: Sci. Technol.* **2**, 035038 (2021).
- [26] J. P. Darby, J. R. Kermode, and G. Csányi, Compressing local atomic neighbourhood descriptors, *Npj Comput. Mater.* **8**, 166 (2022).
- [27] Y. Luo, D. Desai, B. K. Chang, J. Park, and M. Bernardi, Data-driven compression of electron-phonon interactions, *Phys. Rev. X* **14**, 021023 (2024).
- [28] K. Esfarjani and H. T. Stokes, Method to extract anharmonic force constants from first principles calculations,

- Phys. Rev. B* **77**, 144112 (2008).
- [29] F. Zhou, W. Nielson, Y. Xia, and V. Ozoliņš, Compressive sensing lattice dynamics. i. general formalism, *Phys. Rev. B* **100**, 184308 (2019).
- [30] T. G. Kolda and B. W. Bader, Tensor decompositions and applications, *SIAM Rev.* **51**, 455 (2009).
- [31] V. Lebedev, Y. Ganin, M. Rakhuba, I. Oseledets, and V. Lempitsky, Speeding-up convolutional neural networks using fine-tuned cp-decomposition, [arXiv:1412.6553 \[cs.CV\]](https://arxiv.org/abs/1412.6553) (2015).
- [32] T. Lacroix, N. Usunier, and G. Obozinski, Canonical tensor decomposition for knowledge base completion, in *Proceedings of the 35th International Conference on Machine Learning*, Proc. Mach. Learn. Res., Vol. 80, edited by J. Dy and A. Krause (PMLR, 2018) pp. 2863–2872.
- [33] K. Pierce and M. Morales, [arXiv:2502.17683 \[physics.chem-ph\]](https://arxiv.org/abs/2502.17683) (2025).
- [34] Y. Luo, D. Mangtani, S. Peng, J. Yao, S. Kliavinek, and M. Bernardi, Supplemental material.
- [35] In the optimization, $A_i^\xi(l, b\alpha)$ is truncated in real space up to a cutoff r_c large enough for the low-rank IFC tensor $\tilde{\Phi}^{(n)}$ to span all nonzero elements in the full IFC tensor $\Phi^{(n)}$.
- [36] A. Paszke, S. Gross, F. Massa, A. Lerer, J. Bradbury, G. Chanan, T. Killeen, Z. Lin, N. Gimelshein, L. Antiga, A. Desmaison, A. Köpf, E. Yang, Z. DeVito, M. Raison, A. Tejani, S. Chilamkurthy, B. Steiner, L. Fang, J. Bai, and S. Chintala, Pytorch: an imperative style, high-performance deep learning library (Curran Associates Inc., Red Hook, NY, USA, 2019).
- [37] G. Kresse and J. Furthmüller, Efficient iterative schemes for ab initio total-energy calculations using a plane-wave basis set, *Phys. Rev. B* **54**, 11169 (1996).
- [38] G. Kresse and D. Joubert, From ultrasoft pseudopotentials to the projector augmented-wave method, *Phys. Rev. B* **59**, 1758 (1999).
- [39] J. P. Perdew, A. Ruzsinszky, G. I. Csonka, O. A. Vydrov, G. E. Scuseria, L. A. Constantin, X. Zhou, and K. Burke, Restoring the density-gradient expansion for exchange in solids and surfaces, *Phys. Rev. Lett.* **100**, 136406 (2008).
- [40] X. Gonze and C. Lee, Dynamical matrices, born effective charges, dielectric permittivity tensors, and interatomic force constants from density-functional perturbation theory, *Phys. Rev. B* **55**, 10355 (1997).
- [41] R. Peierls, *Quantum Theory of Solids* (Clarendon Press, Oxford, 1955) p. 40.
- [42] J. M. Ziman, *Electrons and Phonons* (Oxford University Press, London, 1960) p. 298.
- [43] A. A. Maradudin and A. E. Fein, Scattering of neutrons by an anharmonic crystal, *Phys. Rev.* **128**, 2589 (1962).
- [44] R. S. Tripathi and K. N. Pathak, Self-energy of phonons in an anharmonic crystal too(δ 4), *Il Nuovo Cimento B* **21**, 289 (1974).
- [45] M. Balkanski, R. F. Wallis, and E. Haro, Anharmonic effects in light scattering due to optical phonons in silicon, *Phys. Rev. B* **28**, 1928 (1983).
- [46] T. Feng and X. Ruan, Quantum mechanical prediction of four-phonon scattering rates and reduced thermal conductivity of solids, *Phys. Rev. B* **93**, 045202 (2016).
- [47] Z. Guo, Z. Han, D. Feng, G. Lin, and X. Ruan, Sampling-accelerated prediction of phonon scattering rates for converged thermal conductivity and radiative properties, *Npj Comput. Mater.* **10**, 31 (2024).
- [48] Coefficient of determination, in *The Concise Encyclopedia of Statistics* (Springer New York, New York, NY, 2008) pp. 88–91.
- [49] X. Ai, Y. Chen, and C. A. Marianetti, Slave mode expansion for obtaining ab initio interatomic potentials, *Phys. Rev. B* **90**, 014308 (2014).
- [50] Y. Chen, X. Ai, and C. A. Marianetti, First-principles approach to nonlinear lattice dynamics: Anomalous spectra in pbte, *Phys. Rev. Lett.* **113**, 105501 (2014).
- [51] R. Drautz, Atomic cluster expansion for accurate and transferable interatomic potentials, *Phys. Rev. B* **99**, 014104 (2019).